Yves Mollet, Matteo Pergolesi, Mathieu Sarrazin, Karl Janssens, Herman Van der Auweraer, Paolo Chiariotti, Paolo Castellini and Johan Gyselinck

Université Libre de Bruxelles
Avenue Franklin Roosevelt 50 (CP165/52)
1050 Brussels
Belgium

Università Politecnica delle Marche
Piazza Roma 22
60121 Ancona AN
Italy

Siemens Industry Software N.V
Interleuvenlaan 68
3001 Leuven
Belgium

Phone: +32 (0) 2 650 26 61
Fax: +32 (0) 2 650 26 53
Email: yves.mollet@ulb.ac.be

Multi-Physical Signature Analysis of Induction Machines under Unbalanced Supply Voltage

Yves Mollet, *Member, IEEE*, Matteo Pergolesi, Mathieu Sarrazin, Karl Janssens, Herman Van der Auweraer, *Member, IEEE*, Paolo Chiariotti, Paolo Castellini, and Johan Gyselinck, *Member, IEEE*

Abstract—This paper investigates the effect of voltage-unbalance fault on current, vibration, acoustic noise and instantaneous power of an open-loop-controlled 1/3 HP and a closed-loop controlled 3 kW induction machine drive. Experimental tests are performed in the form of run-ups and the results are plotted as colormaps to visualize the effect of the unbalance in a large speed range. Based on the observation of these plots, the relevant orders are tracked to compare their evolution with speed, load and unbalance severity, emulated by an increasing resistance inserted on one phase up to the open-phase fault case. It turns out that the analysis of the computed instantaneous power and the estimated RMS current is more suited for a reliable diagnosis in all cases.

Index Terms—Amplitude modulation; Fault detection; Induction motors; Harmonic analysis; Harmonic distortion; Signal detection; Spectral analysis; Colormap; Transient condition; Variable speed drives

I. Introduction

Induction machines (IMs) are used in numerous industry applications, thanks to their simple construction, high reliability and the availability of power converters and efficient control strategies. Among the different types of failures affecting those drives, the largest proportion of occurrences (more than 75 %) in low-voltage applications is related to the bearings, the stator and rotor faults representing each a few percent. The part of stator faults rises to about 35 % for medium- and high-voltage machines, besides about 40 % and 10 % for bearing and rotor faults respectively [1].

For the cases where a failure of the machine may lead to high production losses or even to loss of lives, different monitoring techniques have been developed, among others based on temperature, vibration or current measurements [1], [2]. Such a permanent condition monitoring of an electrical drive generally requires supplementary instrumentation and is therefore too expensive to be implemented in non-critical applications unless for big machines [3]. However, reduced

implementation costs can be achieved by current monitoring, which takes benefit from the current sensors already integrated in the drive for control purpose and overload protection and limits the amount of measurements to be acquired [2], [4].

Using current-signature analysis, a large number of mechanical and electrical faults have been dealt with in literature. Detailed models for several kinds of mechanical faults such as bearing damage, eccentricity and torque oscillations are developed in [3], [5]. The case of broken rotor bars is discussed (among others) in [2], [6]. Electrical measurements are also compared with vibrations ones in [7], [8] to investigate the effects of voltage-unbalance faults on induction motor speed, torque and power.

Besides the classical fast Fourier transform (FFT) more advanced spectral-based techniques, proposing a finer resolution or applicable to noisier signals are reviewed in [2], [9]. Methods tracking the Park's vector module or pattern [10], [11], or the negative-sequence current [12], as well as using Hilbert transform are also proposed [2], [9].

Some time-domain techniques are also listed in [2], such as the analysis of transient currents of line-starting machines. Time-frequency techniques are e.g. based on Wigner distribution, and wavelet and Hilbert-Huang transforms [2], [13].

The present paper focuses on the multi-physical signature analysis of supply voltage unbalance on IMs. Such faults can be caused by a bad connection or a fault in the supply chain of the machine. Open-phase faults can be regarded as a particularly strong unbalance, as the impedance of one phase becomes infinite. They can result, on the one hand, from a broken cable or connection in the supply, the action of a fuse in case of over-current or, on the other hand, from a manufacturing defect or the burnout of a weak point of the winding [14]. In variable-speed drives an open-switch fault in the power converter also leads to a similar behaviour [15].

As accelerometers are sometimes already present for the condition monitoring of other components of the facility and for a more comprehensive understanding of the effect of voltage unbalance, not only the phase current, but also vibration and acoustic noise signals are analysed in this paper. The computed instantaneous power is also investigated, as components are observable in the low-frequency range (e.g. at modulation frequencies) [9], [16]. An indicator, corresponding to the RMS current in balanced conditions and easily computed from the available multiple current measurements in drives is also presented.

Section II presents the frequency content that appears in current and vibration measurements in balanced and unbalanced cases. Section III describes the investigated machines, the respective test benches and associated measurement setups. The experimental results are shown and discussed in Section IV.

II. Main Current Frequency Content in an IM and in case of Balanced and Unbalanced Supply

In the balanced case, the current spectrum is dominated by the supply frequency and its multiples. Higher-frequency components are also present, because of the stator and rotor slotting and magnetomotive force harmonics [17]. The magnetic saturation of the machine is at the origin of a third spatial harmonic of air-gap flux density, rotating at the same speed as the fundamental wave [18] and of components of the rotor currents at three times the slip frequency [2]. Their interaction with the fundamental stator flux causes the apparition of side peaks at $(1 \pm 2s)f_s$ and $(1 \pm 4s)f_s$ in the current spectrum, with f_s and s the stator frequency and the slip. It has to be noted that all those components overlap with frequencies related to broken rotor bars [2]. The third spatial harmonic of the stator flux further interacts with the rotor slots and generates specific slotting frequency components [2], [18].

In case of voltage or impedance unbalance, an inverse-sequence current flows in the stator at frequency $-f_s$, a zero-sequence one only flowing in case of star connection and in presence of the neutral wire. The interaction of positive- and negative-sequence currents gives rise to a torque oscillation at $2f_s$, also visible on the amplitude of the current Park's vector [17]. The spectra of active and reactive power also shows peaks at that frequency, their amplitudes being directly related to the fault severity [16].

The torque oscillation at $2f_s$ causes a speed fluctuation at the same frequency [7], [8], itself generating a modulation of stator currents leading to side peaks at $f_s \pm 2f_s$ [9]. The presence of components at $3f_s$ in the stator currents are confirmed in [16], which also mentions the sensitivity of this harmonic component to magnetic saturation and static eccentricity.

Voltage unbalances also increase the amplitudes of the third-order slotting harmonics, while they are absent in perfectly balanced conditions regarding both machine and supply [17].

It has to be noted that current components at f_s and $3f_s$ and at the third-order slotting harmonics are also generated in case of impedance unbalance and inter-turn short circuits in the machine. However, in case of voltage unbalance only, the amplitude of the terminal voltages presents a component at $2f_s$ [16].

III. Investigated Machines and Test Set-ups

Two test benches are used in the frame of this work: the first one is composed of a 1/3 HP IM coupled with a flywheel; the second one comprises a 3 kW IM coupled with a 3 kW DC machine. The rated values of those induction machines called IM1 and IM2 are listed in Table I.

TABLE I
RATED VALUES OF THE INVESTIGATED IMS

	IM1	IM2
Rated power [kW]	0.249	3
Rated phase-to-phase voltage [V]	190	400
Rated current [A]	2	6.1
Rated frequency [Hz]	50	50
Number of pole pairs	1	2
Rated speed [rpm]	2850	1420

Both IMs are fed by commercial inverters: a Delta VFD-S drive (with a simple scalar control) and an ABB ACS880 drive (with an internal closed-loop direct-torque control) are used for IM1 and IM2 respectively. In both cases an external resistor R_{add} is inserted between the drive and the machine in one phase to emulate a phase unbalance, as presented in Fig. 1 and 2. While the basic open-loop control used for the IM1 allows investigating a large range of unbalances including the case of phase loss by inserting a rheostat in phase c and a switch in phase b, only a 2 Ω resistor is inserted in phase a of the IM2 without causing a tripping of the internal safeties of the more advanced ABB drive.
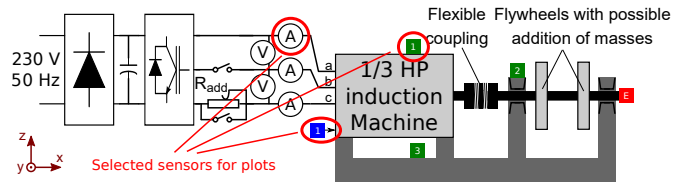

Fig. 1. IM1 test bench, including the external resistor and the position of the sensors. The encoder, accelerometers and microphone are represented in red, green and blue respectively.
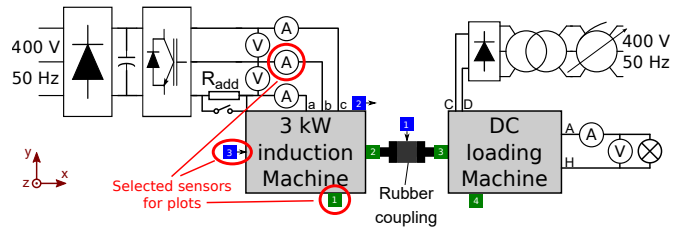

Fig. 2. IM2 test bench, including the external resistor and the position of the sensors. The accelerometers and microphones are represented in green and blue respectively.

In the case of the IM2 test bench loaded tests are performed by connecting the DC machine to resistors, while keeping the excitation current constant. The resulting load torque is proportional to speed and corresponds to the rated load at rated speed.

All phase currents and two phase-to-phase voltages at the machine terminals are acquired using an LMS SCADAS system, as well as the vibration and acoustic noise measurements at the locations mentioned in Fig. 1 and 2. A 5000 pulse-per-turn and a 1 pulse-per-turn encoder are used for the IM1 and IM2 benches respectively.

The instantaneous power p and current indicator $I_{rms}^{\#}$ (equal to the rms current in balanced sinusoidal conditions) are computed from the measured signals as follows:

$$p = v_a \cdot i_a + v_b \cdot i_b + v_c \cdot i_c, \qquad (1)$$

$$I_{rms}^{\#} = \sqrt{\frac{i_a^2 + i_b^2 + i_c^2}{3}}, \qquad (2)$$

with v_a, v_b and v_c, and i_a, i_b and i_c the three phase-to-neutral voltages and currents. As two phase-to-phase voltages v_{ab} and v_{bc} are measured, the phase-to-neutral voltages v_a, v_b and v_c can be retrieved using the following equations:

$$v_a = \frac{v_{ab} - v_{ca}}{3}, v_b = \frac{v_{bc} - v_{ab}}{3}, v_c = \frac{v_{ca} - v_{bc}}{3}, \qquad (3)$$

with $v_{ca} = -v_{ab} - v_{bc}$.

IV. EXPERIMENTAL RESULTS

Contrary to classical steady-state tests, run-ups enable to investigate important ranges of working points of the machine, highlighting the influence of speed on results while exciting a large range of frequencies [19]. Speed ramps are therefore performed on both test benches from 0 rpm to rated speed in balanced and unbalanced cases. While a simple frequency ramp is generated by the Delta converter on the 1/3 HP IM, a speed ramp is imposed to the 3 kW machine through the closed-loop controller of the ABB drive.

Testing in transient conditions allows to use a more advanced signal processing technique compared to the classical fast-Fourier transform (FFT). The acquired signals are first decomposed into a succession of short-time ones by using a sliding window, for which steady-state conditions can be assumed due to the slow evolution of speed. An FFT is performed on each resulting signal and each obtained spectrum is then associated to the time at the middle point of the window. Overlapping windows are here used to increase time resolution, the quarter of window length being chosen as time shift between two consecutive windows.

However, instead of superposing the spectra on a 3D plot showing the amplitude in function of frequency and time, as explained in [20], the time axis is here converted into a speed axis according to the defined speed profile. However, due to possible speed oscillations present in the original signal, these results are, in practice, sorted by increasing speed and interpolated according to a regularly growing speed profile (with a speed resolution of 1 rpm). The speed value used for this sorting is the measured speed at the middle point of the considered window. Results are finally plotted as colormaps to allow for a global visualization of frequency content in function of speed.

A. IM1 test bench

The colormaps of phase current, radial vibration and acoustic noise (see selected sensors in Fig. 1), on the one hand, and of the $I_{rms}^{\#}$ indicator and instantaneous power on the other hand, corresponding to a run-up of IM1 with balanced supply at no-load are presented in Fig. 3 and 4 respectively. Results are plotted in dB scale, the references being 1 A, 1 m/s^2, 20 μPa (i.e. dB SPL), 1 A and 1 W respectively. The A-weighted dB are not used here to characterize sound pressure levels for easier comparison with other quantities. The acceleration rate, sampling frequency and window length are 16.67 rpm/s, 512 Hz and 4096 samples respectively. The frequency and speed resolutions of the colormaps are 0.125 Hz and 1 rpm respectively.
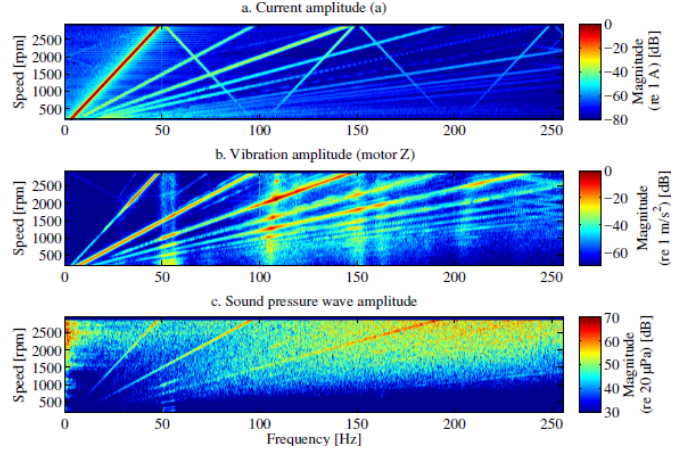

Fig. 3. Colormaps of the current, vibration and sound-pressure wave obtained during a run-up test on IM1 (balanced case).
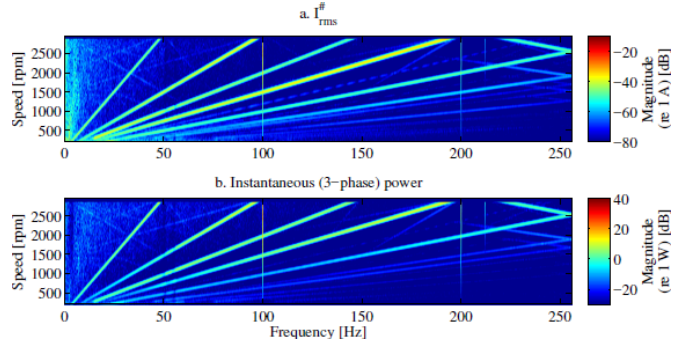

Fig. 4. Colormaps of the $I_{rms}^{\#}$ indicator and instantaneous power during a run-up test on the 1/3 HP machine (balanced case).

The current plot of Fig. 3 essentially shows the current orders (i.e. the fundamental and harmonics), forming oblique green to red lines going from the origin {0 Hz, 0 rpm} to {50 Hz, 3000 rpm}, {100 Hz, 3000 rpm}, {150 Hz, 3000 rpm} etc. Some lines having their origin at {100 Hz, 0 rpm} and {200 Hz, 0 rpm} are related to the interaction of current orders with the residual oscillation of the DC-bus voltage at 100 Hz, fed by the grid through a 1 phase diode bridge.

The current orders are also visible on the vibration and acoustic-noise plots, due to generation of magnetostrictive and Maxwell forces in the machine [21]. The associated phenomena are the trend of the iron to be deformed under a magnetic field and the attraction forces between stator and rotor according to the maximum-flux principle respectively.

Acoustic noise is produced by the resulting radial deflection of the yoke, which is proportional to the square of the magnetic induction [21]. This probably explains the globally higher amplitude of the second current order compared to the first one in the vibration plot and the relative dominance of even current orders in the acoustic-noise plot. An amplification of the orders close to 50 Hz and in a frequency range from 100 to 150 Hz may be attributed to interaction with structural resonances. A modal analysis will be performed in the future to confirm this hypothesis.

The multiplication of the dominating odd current harmonics with each other or with voltage components leads to the generation of a DC component and of dominating even current orders in the colormaps of $I_{rms}^{\#}$ and instantaneous power in Fig. 4. This can be easily verified, as applying the Simpson's formulae to the product of two sine waves at odd multiples results in a sum of even multiples of the fundamental frequency, a DC component being present in the case of a product of two sine waves of identical frequency. The oblique lines with negative slopes on the last 20 % of the frequency range of the plots in Fig. 4 are related to aliased content, since the cut-off frequency of the anti-aliasing filter of the SCADAS is set to 80 % of the Nyquist frequency.

The corresponding colormaps obtained while inserting a 12.9 Ω resistor in phase c are presented in Fig. 5 and 6 respectively. As expected, the introduction of the unbalance increases the amplitude of the third order in the current plot, while other odd orders are also amplified. On the $I_{rms}^{\#}$ and instantaneous-power plots the amplitude of the even current orders (essentially orders 2 and 4) are increased compared to the balanced case. This can be explained once again using Simpson's formulae, based on the interaction of the additional inverse-sequence and increased third harmonic current components with the fundamental current or voltage component. For the same reasons an increase amplitude of the second current order is also expected on the vibration and acoustic-noise plots, but turns out to be less visible and highly dependent on the working conditions in practice.
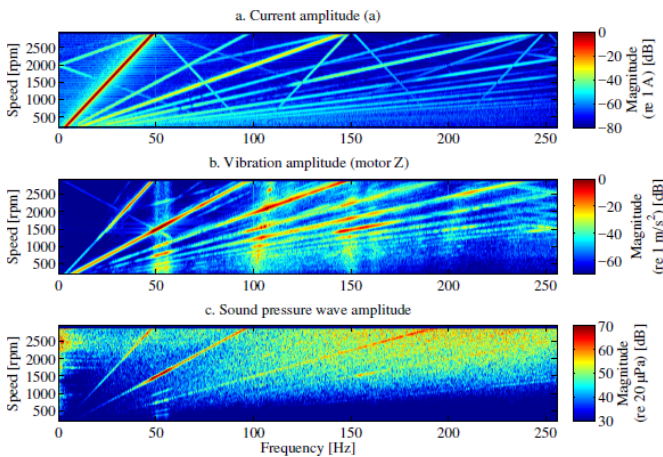

Fig. 5.   Colormaps of the current, vibration and sound-pressure wave obtained during a run-up test on IM1 with 12.9 Ω inserted in phase c.
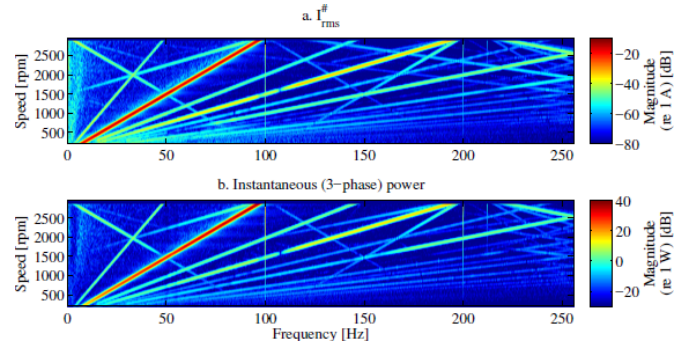

Fig. 6.   Colormaps of the $I_{rms}^{\#}$ indicator and instantaneous power during a run-up test on IM1 with 12.9 Ω inserted in phase c.

Based on the observations above, the main varying stator-frequency orders in case of voltage unbalance (i.e. the third order of phase current and the second one of the $I_{rms}^{\#}$ indicator and instantaneous power) are tracked in Fig. 7 for run-ups with IM1 in balanced case, for two different values of inserted resistance and in case of open phase fault. For that purpose the supply frequency and phase angle are first computed from the measured voltages by means of a PLL. These values are then used to resample the acquired signals according to a regularly increasing stator electrical angle. No tracking of the vibration and acoustic-noise orders is presented in this paper, as the difference between balanced and unbalanced cases is less visible and only clear in limited speed ranges.
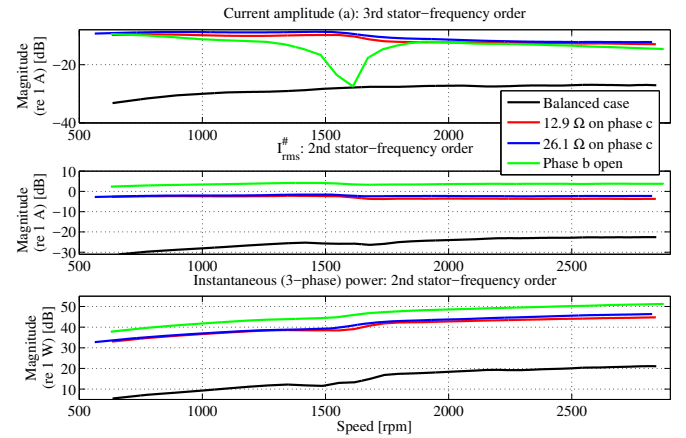

Fig. 7.   3rd stator-frequency order of the current and 2nd stator-frequency orders of the $I_{rms}^{\#}$ indicator and instantaneous power during a run-up on IM1 for balanced case and different unbalance severities.

Regarding the current plot in Fig. 7, the difference in amplitude is relatively limited between unbalanced cases and no regular evolution can be observed with unbalance severity, whereas all values are much higher than in the balanced case. The second orders of the $I_{rms}^{\#}$ indicator and of the instantaneous power have a relatively constant and continuously increasing profile with speed respectively. Regarding the effect of unbalance severity, a more regular evolution appears, with, however, very limited difference of

amplitude between both intermediate cases. The more regular observed evolutions of the $I_{rms}^{\#}$ indicator or the instantaneous power with respect to speed and severity show the advantage of using them for unbalance diagnosis, since they rely on several electrical measurements and therefore give a more global information on the machine behaviour than a single current, vibration or acoustic noise measurement.

B. IM2 test bench

Similarly to the case of IM1 the colormaps of phase current, radial vibration and acoustic noise (see selected sensors in Fig. 2), on the one hand, and of the $I_{rms}^{\#}$ indicator and instantaneous power on the other hand, corresponding to a run-up of IM2 with balanced supply at load are presented in Fig. 8 and 9 respectively. Electrical and mechanical measurements are acquired at 25.6 kHz and 12.8 kHz respectively for an acceleration rate of 75 rpm/s. Due to the higher run-up slope compared to the tests on IM1, the acquisition time is smaller and therefore a longer window length (16384 samples) is set to avoid a too coarse frequency resolution of the colormaps (equal to 1.5625 Hz for this test bench). As it is related to the post-processing, the speed resolution remains the same as for IM1, i.e. 1 rpm. The maximum frequency of the colormaps is set to 1 kHz to zoom on the main relevant current orders.
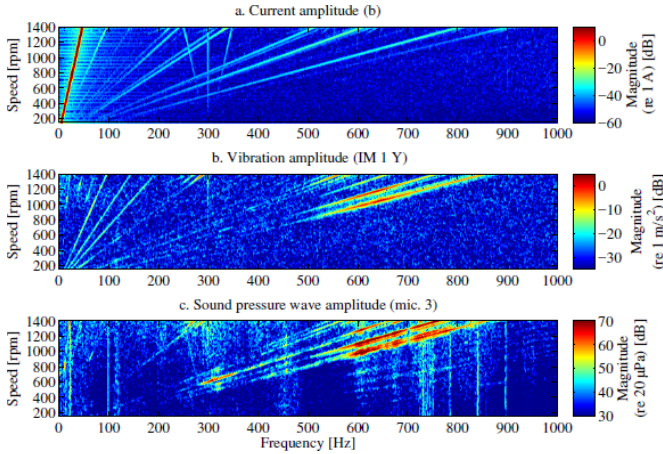

Fig. 8. Colormaps of the current, vibration and sound-pressure wave obtained during a run-up test on IM2 (balanced case) at constant excitation and load resistance fed by the DC machine (corresponding to the rated load at rated speed).

The plots of Fig. 8 are similar to the ones of Fig. 3. However, only non-triplen odd orders, i.e. of $6k\pm1$ order ($k \in \mathcal{Z}$), can be seen in the current plot. The number of visible current orders is also limited in the vibration and acoustic-noise plots. Furthermore, as the drive of that bench is fed by a three-phase diode bridge, oblique lines having their origin at {300 Hz, 0 rpm} replace the ones starting at {100 Hz, 0 rpm} and {200 Hz, 0 rpm} in the case of IM1.

The fact that only the second order and of the orders multiple of six are essentially visible in the colormaps of $I_{rms}^{\#}$ and instantaneous power in Fig. 9 has to be attributed
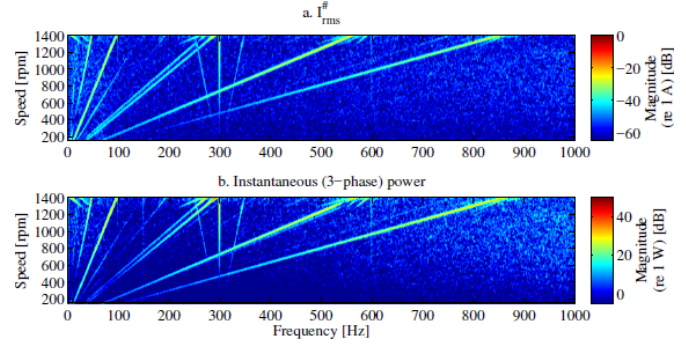

Fig. 9. Colormaps of the $I_{rms}^{\#}$ indicator and instantaneous power during a run-up test on IM2 (balanced case) at constant excitation and load resistance fed by the DC machine (corresponding to the rated load at rated speed).

to the reduced amplitudes of current harmonics compared to the case of IM1.

The corresponding colormaps obtained with a 2 Ω resistor in phase a are presented in Fig. 10 and 11 respectively. The unbalanced supply of IM2 leads to very similar results as for IM1, except that the amplification of the harmonic is is here much more visible in the current plot.
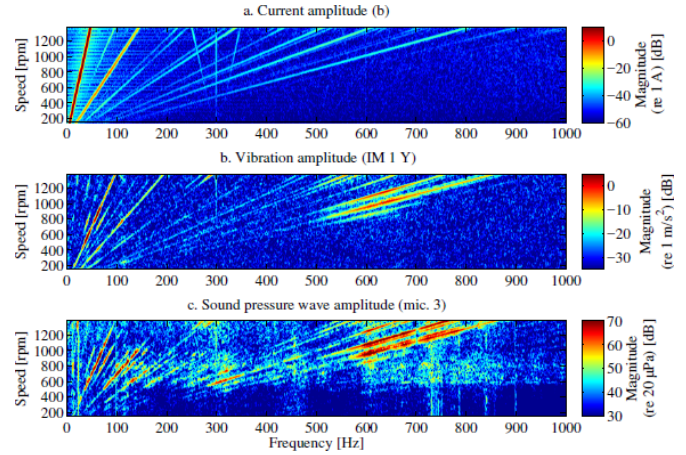

Fig. 10. Colormaps of the current, vibration and sound-pressure wave obtained during a run-up test on IM2 with 2 Ω inserted in phase a at constant excitation and load resistance fed by the DC machine (corresponding to the rated load at rated speed).

The same orders as for the IM1 are tracked for IM2 and plotted in Fig. 12. The balanced case and the addition of a 2 Ω resistance in phase a without and with load are considered.

A relative high difference (about 20 to 25 dB) between the amplitude of the third current harmonic in unbalanced and balanced loaded cases can be observed in Fig. 12. This difference is also roughly present in the second order of the $I_{rms}^{\#}$ indicator and instantaneous power. However, this cannot be said for the no-load case, for which the difference between unbalanced and balanced conditions decreases to 5 to 10 dB in the second order of the $I_{rms}^{\#}$ indicator and instantaneous power. Furthermore, the amplitudes of the observed orders are globally higher with load in case of unbalance, while the opposite can be seen in the balanced case.
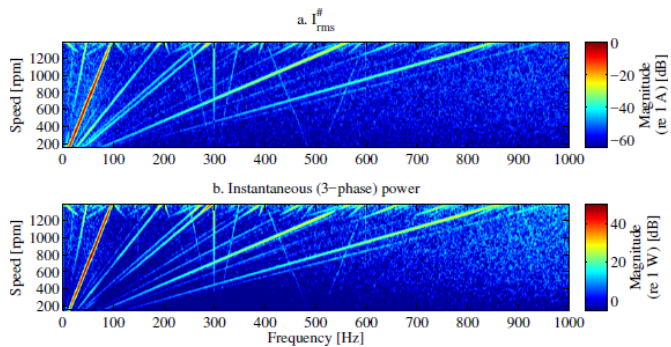
Fig. 11. Colormaps of the $I_{rms}^{\#}$ indicator and instantaneous power during a run-up test on IM2 with 2 Ω inserted in phase a at constant excitation and load resistance fed by the DC machine (corresponding to the rated load at rated speed).
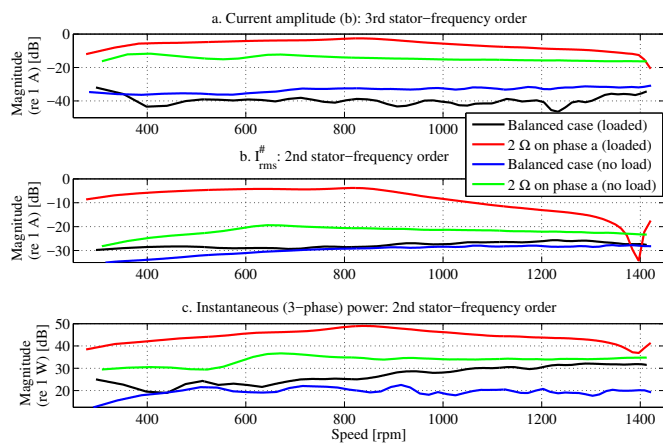

Fig. 12. 3rd stator-frequency order of the current and 2nd stator-frequency orders of the $I_{rms}^{\#}$ indicator and instantaneous power during a run-up on IM2 for balanced and unbalanced conditions for both no-load and load cases.

These observations may be partly explained by the low value of resistance in IM2 compared to IM1, which creates a limited unbalance at no load. The use of a closed-loop controller for IM2 may also induce a global reduction of the unbalance compared to the open-loop one of IM1 as it tends to compensate for disturbances [2]. However, the addition of a load globally increases the observed differences between balanced and unbalanced cases, since the higher current flowing through the additional resistor increases the voltage unbalance in load case.

V. CONCLUSIONS

The detectability of voltage unbalances through multi-physical signature analysis on a 3 kW and a 1/3 HP IM has been experimentally investigated by comparing the frequency content of phase current, vibration, acoustic noise, $I_{rms}^{\#}$ indicator and instantaneous power. Results for run-ups in various test conditions have been plotted as colormaps and as amplitude of the relevant orders in function of speed.

Results on both test benches show an increase of the third current harmonic and of the second current order in vibration, acoustic noise, instantaneous power and $I_{rms}^{\#}$ indicator under voltage unbalance. Other odd harmonics in the current plot and the fourth current order in the other plots are also affected, but in a limited extent.

The behaviour of the vibration and acoustic noise turns out to be highly dependent on the bench and on speed, contrary to the instantaneous power and the $I_{rms}^{\#}$ indicator, which have a more homogeneous reaction, thanks to their global character. The current has an intermediate behaviour, essentially depending on the machine, but less on the working conditions. Therefore, the use of the $I_{rms}^{\#}$ indicator may be a convenient way to detect voltage unbalances, as it can further use current sensors already installed in the drive.

In future work, the impact of voltage unbalance associated with different control strategies will be further investigated, as well as other fault types, such as mass unbalance or misalignment. A modal analysis of the machines will also be performed to better characterize the structural resonances.

REFERENCES

[1] P. Tavner, "Review of condition monitoring of rotating electrical machines," *IET Electric Power Applications*, vol. 2, no. 4, pp. 215 – 247, 2008.

[2] A. Bellini, F. Filippetti, C. Tassoni, and G.-A. Capolino, "Advances in Diagnostic Techniques for Induction Machines," *Industrial Electronics, IEEE Transactions on*, vol. 55, no. 12, pp. 4109–4126, 2008.

[3] M. Blödt, P. Granjon, B. Raison, and G. Rostaing, "Models for Bearing Damage Detection in Induction Motors Using Stator Current Monitoring," *IEEE Transactions on Industrial Electronics, Institute of Electrical and Electronics Engineers*, vol. 55, no. 4, pp. 1813–1822, 2008.

[4] Y. Gritli, A. Bellini, C. Rossi, D. Casadei, F. Filippetti, and G.-A. Capolino, "Condition monitoring of mechanical faults in induction machines from electrical signatures: Review of different techniques," in *2017 IEEE 11th International Symposium on Diagnostics for Electrical Machines, Power Electronics and Drives (SDEMPED)*. Tinos, Greece: IEEE, 2017, pp. 77–84.

[5] M. Blödt, "Condition Monitoring of Mechanical Faults in Variable Speed Induction Motor Drives Application of Stator Current Time-Frequency Analysis and Parameter Estimation," Ph.D. dissertation, Institut National Polytechnique de Toulouse, Toulouse, France, 2006.

[6] F. Filippetti, G. Franceschini, C. Tassoni, and P. Vas, "AI techniques in induction machines diagnosis including the speed ripple effect," *IEEE Transactions on Industry Applications*, vol. 34, no. 1, pp. 98–108, 1998.

[7] D. Mirabbasi, G. Seifossadat, and M. Heidari, "Effect of unbalanced voltage on operation of induction motors and its detection," in *2009 International Conference on Electrical and Electronics Engineering - ELECO 2009*. Bursa, Turkey: IEEE, 2009, pp. 189–192.

[8] G. R. Bossio, C. H. De Angelo, P. D. Donolo, A. M. Castellino, and G. O. Garcia, "Effects of voltage unbalance on IM power, torque and vibrations," in *2009 IEEE International Symposium on Diagnostics for Electric Machines, Power Electronics and Drives, SDEMPED 2009*, no. 3. Cargèse, France: IEEE, 2009.

[9] M. El Hachemi Benbouzid, "A review of induction motors signature analysis as a medium for faults detection," *Industrial Electronics, IEEE Transactions on*, vol. 47, no. 5, pp. 984 – 993, 2000.

[10] I. Y. Önel and M. E. H. Benbouzid, "Induction motor bearing failure detection and diagnosis: Park and concordia transform approaches comparative study," in *IEEE IEMDC 07*, no. 2, pp. 1073–1078.

[11] ——, "Induction motors bearing failures detection and diagnosis using a RBF ANN park pattern based method," *International Review of Electrical Engineering*, vol. 3, no. 1, pp. 159–165, 2008.

[12] J. Zafar and J. Gyselinck, "CUSUM based Fault Detection of Stator Winding Short Circuits in Doubly-Fed Induction Generator based Wind Energy Conversion Systems," in *International Conference on Renewable Energies and Power Quality (ICREPQ'10)*, Granada, 2010.

[13] E. H. El Bouchikhi, V. Choqueuse, and M. Benbouzid, "Induction Machine Diagnosis using Stator Current Advanced Signal Processing," *International Journal on Energy Conversion*, vol. 3, no. 3, pp. 76–87, 2015.

[14] L. Szabó and M. Ruba, "On fault tolerance increase of switched reluctance machines," in *IEEE EUROCON 2009, EUROCON 2009*. St.-Petersburg, Russia: IEEE, 2009, pp. 734–739.

[15] J. F. Marques, J. O. Estima, N. S. Gameiro, and A. J. Marques Cardoso, "A New Diagnostic Technique for Real-Time Diagnosis of Power Converter Faults in Switched Reluctance Motor Drives," *IEEE Transactions on Industry Applications*, vol. 50, no. 3, pp. 1854–1860, 2014.

[16] M. Drif and A. J. Marques Cardoso, "Stator Fault Diagnostics in Squirrel Cage Three-Phase Induction Motor Drives Using the Instantaneous Active and Reactive Power Signature Analyses," *IEEE Transactions on Industrial Informatics*, vol. 10, no. 2, pp. 1348–1360, 2014.

[17] R. Sharifi and M. Ebrahimi, "Detection of stator winding faults in induction motors using three-phase current monitoring," *ISA Transactions*, vol. 50, no. 1, pp. 14–20, 2011.

[18] S. Nandi, "A detailed model of induction machines with saturation extendable for fault analysis," *IEEE Transactions on Industry Applications*, vol. 40, no. 5, pp. 1302–1309, 2004.

[19] M. Sarrazin, S. Gillijns, K. Janssens, H. Van Der Auweraer, and K. Verhaeghe, "Vibro-acoustic measurements and techniques for electric automotive applications," in *INTER-NOISE and NOISE-CON Congress and Conference Proceedings. Institute of Noise Control Engineering*, Melbourne, Australia, 2014, pp. 5128–5137.

[20] E. Cabal-Yepez, A. G. Garcia-Ramirez, R. J. Romero-Troncoso, A. Garcia-Perez, and R. A. Osornio-Rios, "Reconfigurable monitoring system for time-frequency analysis on industrial equipment through STFT and DWT," *IEEE Transactions on Industrial Informatics*, vol. 9, no. 2, pp. 760–771, 2013.

[21] J. Le Besnerais, "Fast prediction of variable-speed acoustic noise due to magnetic forces in electrical machines," *Proceedings - 2016 22nd International Conference on Electrical Machines, ICEM 2016*, no. July, pp. 2259–2265, 2016.

VI. Biographies

Yves A. B. Mollet received the master in industrial engineering from the Haute Ecole Léonard de Vinci (ECAM), in 2010 and the Ph.D. in engineering sciences and technology at the Université Libre de Bruxelles (ULB), in 2017 (both in Brussels, Belgium). He is now a researcher at the ULB and at Siemens Industry Software (Leuven, Belgium). His main research topics concern fault detection and noise and vibrations in electrical machines and drives.

Matteo Pergolesi is currently a student mechanical engineering at "Università politecnica delle Marche". In August 2017 he joined the Simulation and Test Solutions department, Digital Factory, Product Lifecycle Management, Siemens Industry Software N.V. in order to accomplish his master thesis. During the internship he dealt with rotating machinery condition monitoring through multi-physical signature analysis.

Mathieu M. Sarrazin (male) holds a M.Sc. in Electromechanical-electrotechnical Engineering (2009) from the University of Gent Campus Kortrijk and a second M.Sc. in Mechanical Engineering, minor automotive (2012) from the KU Leuven. Since 2012, he is part of LMS International, now known as Siemens Industry Software (SISW). He has 6 years of experience in the applied research. In 2014, he received a unique Siemens Technology Award. Currently, he is a R&D manager and responsible for the definition, planning, managing and execution of research projects related to electro-mechanical drivetrains, model-based system testing, hybrid, electrical and autonomous vehicles, mechatronic systems, system identification, converter-machine interactions, control system strategies and condition monitoring.

Karl Janssens received his Engineer diploma (1995) and PhD degree (1999) from the Katholieke Universiteit Leuven, Belgium. In 2001, he joined LMS International, an engineering innovation company, developing advanced testing and simulation tools for mechatronic product design. LMS International became part of Siemens in 2013. He has more than 15 years of experience in the areas of rotating machinery testing, signal processing, noise source identification, transfer path analysis and sound engineering. At present, he is RTD Division Manager, responsible for research and technology innovation related to testing.

Herman van der Auweraer (M'77) received the M.Sc. degree in electronic engineering (1980) and the Ph.D. degree in engineering science (1987) from the KU Leuven, Belgium. In 1986, he joined LMS International, Leuven, one of the earliest KU Leuven spin-offs, developing advanced testing and simulation tools for mechatronic product design engineering. LMS became part of Siemens in 2013. His research focus is acoustics, sound quality, and system identification. At present, he is Research Director, responsible for the company's technology strategy. Furthermore, he is affiliated to KU Leuven as part-time Professor.

Paolo Chiariotti received his MsC in in Mechanical Engineering (2007) and PhD degree in Mechanical Engineering and Management (2011) from Università Politecnica delle Marche (UNIVPM), Italy. He joined the Mechanical and Thermal Measurement Group at UNIVPM in 2007 and since then has been working in developing measurement procedures, devices, and signal processing methods in the fields of non-contact vibration for structural dynamic and NDT, array acoustics, sound engineering, transfer path analysis and machine condition monitoring. At present, he is Research Associate at UNIVPM.

Paolo Castellini received the PhD degree in 1996 at University of Padova, Italy. In 1997, he joined the Mechanical Department of Ancona, as an researcher and in 2011 become Associate Professor at the Department of Industrial Engineering and Mathematical Sciences at the Polytechnic University of Marche, where he teaches Mechanical and Thermal Measurements and Testing. Prof. Paolo Castellini has more than 24 years activity in the development and application of instrumentation for mechanical measurements in dynamic analysis and vibro-acoustic. He is part of the executive committee of the "International Conference on Vibration Measurements by Laser Techniques: Advances and Applications", in Ancona, which is organised every two years. Paolo Castellini was active in several EU funded project. He was the coordinator of a CleanSky EU project and he is the coordinator of a European Industrial Doctorate. His research interests are related to non-contact mechanical measurement techniques, mainly based on laser and microphone arrays. He is author of about hundred papers in International reviews and conferences.

Johan J. C. Gyselinck (M05) received the M.S. degree in electrical and mechanical engineering and the Ph.D. degree in applied sciences from Ghent University, Gent, Belgium, in 1991 and 2000, respectively. From 2000 to 2004, he was a Postdoctoral Researcher at the Applied and Computational Electromagnetics research unit of the University of Liège, Liège, Belgium. He is currently an Associate Professor with the Université Libre de Bruxelles, Brussels, Belgium, and his research mainly concerns the numerical computation of magnetic fields, the simulation and control of electrical machines and drives, and renewable energy systems.